

CHILD POSES IN CHILD RESTRAINT SYSTEMS RELATED TO INJURY POTENTIAL: INVESTIGATIONS BY VIRTUAL TESTING

Lex van Rooij, Christelle Harkema, Ronald de Lange, Kate de Jager, Marian Bosch-Rekvelde, Herman Mooi

TNO Science and Industry
The Netherlands
Paper Number 05-0373

ABSTRACT

In Europe approximately 1250 children younger than 15 years of age die in traffic each year. The number of children severely injured in traffic is dramatically higher. Within the ECE-R44 regulation the safety of children in cars has been regulated by means of certification of child restraint systems (CRS). Much has been achieved, but further reduction of injuries seems possible. The ECE-R44 regulation provides a simplified set up and test configuration, that may be different from the real-world environment in which a child is injured.

In this study, a virtual testing approach was followed to explore the effect of one particular aspect, i.e. the posture of a child in a CRS, on the injury potential in a typical car crash. The investigation focussed on the vulnerable child population seated in ECE-R44 Group I seats. A photo-study was performed with 10 children in the age group from one to three years. Their positions were recorded on short and longer drives. Few children remained seated in the standard position. Most children slouched, slanted and turned their head and rested it on the side-support of the CRS. Extreme positions such as leaning forward, escaping from the harness or holding feet were observed. In the MADYMO simulation environment a non-deforming finite element model of a CRS was combined with multi-body models of Q1.5 and Q3 dummies and of human child models representing 1.5 and 3-year-olds. They were set up in realistic poses. The dummy models were adapted to enable these poses, while the human models were used to compare the biofidelity performance. From the simulated response between the ECE-R44 prescribed position and various common and extreme positions children were found to be in, it was shown that children are at an increased risk in relatively common positions. High lateral neck loads were observed in slanted positions, while correctly restrained children that managed to escape from their shoulder harness sustained large amounts of head excursion. Virtual testing was shown to be a valuable tool to predict trends in situations that are more closely related to the actual automotive environment than current regulations or hardware testing do.

INTRODUCTION

In the 15 countries that comprised the European Union until 2005, approximately 1250 traffic fatalities were recorded among children up to 15 years of age in the year 2002 [EU, 2005]. Approximately half of these fatalities were from child occupants, the rest from pedestrian or cyclists. Although the number of fatalities is relatively small compared to adult fatalities, the number of injuries children sustain is dramatically larger.

Serious or fatal injuries in child occupants have various causes. The use of an appropriate child restraint system (CRS) is a key requirement for protecting a child. A CRS prevents the child to impact vehicle interior structures and it ensures a belt restraint condition that is designed specifically for the smaller anthropometry of a child. However, the CRS needs to be installed properly, which often is difficult to do and hence causes potentially dangerous situations [Quintero del Rio, 1997]. In addition, child restraint systems are designed for a specific range of body weight or length. When a child is seated in a CRS that is inappropriate for its weight or length, potentially hazardous restraint conditions may exist. Parents are often prone to prematurely graduate their child to a larger seat, which causes an inappropriate belt fit. The latter may result in submarining, the lap belt cutting into the abdomen while the child's pelvis slides underneath.

Even when the proper CRS is installed in the vehicle and the child is positioned correctly with no slack in any of the belts, a serious injury risk may exist. Current CRS designs allow children a certain amount of freedom to move around in their seats. Meissner et al. showed that children seated in booster seats have a large tendency to move with respect to their CRS and to move the belt restraint around [Meissner, 1994]. Whether any posture other than the standard posture a child is in when positioned in the CRS has an effect on the injury risk is unknown.

The currently existing test method for evaluating the performance of child restraint systems in the EU is ECE-R44 [ECE, 1998]. Within this regulation a frontal impact sled test is performed at an impact speed of 50 km/h. A child dummy that is appropriate for the tested seat is installed properly, while all belt restraints are pretensioned. Since no vehicle interior is implemented, no information is provided on a possible interaction of the child with the vehicle. Euro-NCAP installs child restraints on the rear seat of vehicles in their full-scale crash tests in order to evaluate the child safety performance of the vehicle in both frontal as well as side impact. However, the vehicle manufacturer is free to choose any CRS and will therefore always choose the seat with the best performance rating, thus eliminating the gross of seats on the market. Various consumer testing programs are being developed in order to ensure safer CRS designs that are easier to install and will reduce injury risk of child occupants.

Currently, within both ECE-R44 and Euro-NCAP testing child dummies of the TNO P-series are used. While these dummy designs have been successful in terms of reproducibility and durability, the biofidelity of their response is limited. A new series of child dummies, the Q-family, was designed in order to overcome the lack of biofidelity. Currently, the dummy performance is being tested in a research environment [de Jager, 2005].

Virtual testing, or numerical simulation, is a useful method for extrapolating beyond currently existing test methods and dummies. While current experimental test methods are limited to hardware dummies and a limited amount of test conditions, parametric simulation studies are virtually unlimited in size and amount of parameters. Simulations are only valid within the range they are validated for, but extending outside the range of validation might be useful in showing possible trends.

The objective of this study was to investigate the effect of various poses on the injury response of children in child restraints. In a virtual testing environment first of all the model setup needed to be created. Human surrogate models of two anthropometries were developed; 1.5 and 3-year-old. Dummy models of the Q-family were developed and validated against component tests. Human child models were generated in order to compare the biofidelity response of the models. In order to find out which poses were common and which poses were extreme a photo study was performed. Common poses and some extreme poses were simulated in a crash environment model with dummy and human geometry in order to

indicate a potential increase of injury risk in poses different than the standard one.

METHODS

In the methods section, first the development and validation of the modeling environment needed for the posture study will be discussed. Secondly, the posture study itself will be discussed, subdivided into photo study and simulation study.

Q3 dummy model development

A multi-body model of the latest version of the Q3 hardware dummy [de Jager, 2005] was created based on a pre-existing Q3 ellipsoid dummy model [MADYMO, 2004]. The model consisted of 32 rigid bodies that were interconnected by 32 kinematic joints. Mass and inertia properties were attributed to the rigid bodies, while force models were implemented in the joints. The outer geometry of the model was represented by 40 ellipsoids and 4 cylinders for which contact characteristics were defined. The resulting model is shown in figure 1.

In order to compare properties of the developed Q3 dummy model with the actual hardware dummy, the segment mass distributions between various body parts is shown in table 1 for the production dummy specifications as well as for the dummy model. The total mass of the dummy was approximately 14.5 kg.

Table 1: Segment mass distribution of Q3 dummy and dummy model.

Segment mass [g]	Q3 product specs.	Q3 model
Head	2784	2784
Neck	382	381
Torso Upper	1976	2047
Torso Lower	4032	4245
Arms Upper	750	760
Arms Lower	728	740
Legs Upper	2000	1980
Legs Lower	1542	1540
Suit	390	0
Total	14584	14477

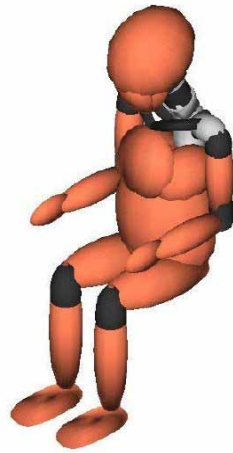


Figure 1. The MADYMO Q3 dummy model.

The Q3 dummy model was developed to represent the Q3 hardware dummy, allowing for validation against component test data of the current hardware dummy.

Q1.5 dummy model development

A Q1.5 dummy model was developed to represent the Q1.5 hardware dummy. This dummy can be applied in both Group 0+ as well as Group I child restraint evaluation and is therefore seen as an important dummy in the Q-family. Geometrical data of the Q1.5 dummy was obtained from a CT scan database that was processed with visualization package Mimics [Mimics, 2005]. From this database external anthropometric dimensions were computed as well as internal geometrical landmarks such as joint locations. A cross-section scan of the Q1.5 dummy in the frontal plane is shown in figure 2.

The Q1.5 dummy model was developed by anthropometrical scaling of the Q3 dummy model, followed by manual corrections to obtain correct segment mass distributions. The MADYMO/Scaler module scaled based on a set of 35 anthropometric parameters, such as seated height and hip breadth [MADYMO, 2004]. This set was defined for the Q3 dummy model based on the dimensions of the model. For the Q1.5 dummy model, the set of parameters was derived from the CT database. From these two anthropometric datasets, scaling parameters were determined for 14 body regions in three directions. The Q1.5 dummy model was created by applying scaling rules, with the obtained scaling parameters, to dimensions, mass and inertia, stiffness and damping parameters. The resulting dummy model resembled the Q1.5 model in terms of anthropometry and internal joint locations. The resulting dummy model is shown in figure 2.

In order to make the model comply with the segment mass distributions as specified for the production dummy, the mass and inertia parameters of the rigid bodies were altered. A comparison of segment mass distribution between actual dummy and developed model is provided in table 2.

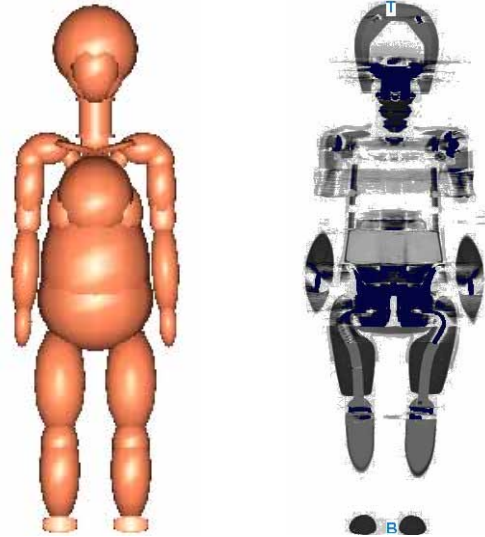


Figure 2. The MADYMO Q1.5 dummy model and CT scan of actual dummy.

The mass of the actual Q1.5 dummy neck did not differ from the mass of the Q3 dummy neck. An identical neck design was used for both dummies. Accordingly, scaling rules in the neck assembly of the model were suppressed in order to leave the neck of the model unchanged.

Table 2: Segment mass distribution of Q1.5 dummy and dummy model.

Segment mass [g]	Q1.5 product specs.	Q1.5 model
Head	2400	2400
Neck	382	381
Torso Upper	1324	1336
Torso Lower	3408	3658
Arms Upper	575	556
Arms Lower	620	625
Legs Upper	1140	1152
Legs Lower	922	899
Suit	305	0
Total	11076	11007

The Q1.5 dummy model, as developed by scaling from the Q3 dummy model, resembled the actual Q1.5 dummy as far as anthropometry,

internal dimensions and mass distributions goes. The stiffness values of soft tissue contact models and kinematic joint stiffness were scaled from the Q3 model. Component validation was needed to show validity of the applied scaling technique.

Dummy model component validation

Validation of the dummy models was performed against component tests as specified in the dummy design requirements [FTSS, 2003]. No full scale sled test data was available, hence no validation on the whole body dummy was performed.

Q3 dummy model – An overview of validation simulations performed for the Q3 dummy model is shown in table 3. For all test conditions corridors or peak response and timing of peak were available, as defined for assessing dummy biofidelity. For frontal and lateral head drop tests, for frontal thorax impactor tests and for lumbar flexion tests hardware dummy test data was available, in addition to corridor requirements.

Table 3: Overview of validation performed on Q3 dummy model.

Test description	Specifications	
Head		
Frontal drop*	Drop height	130 mm
Frontal drop*	Drop height	376 mm
Lateral drop*	Drop height	130 mm
Lateral drop*	Drop height	200 mm
Neck		
Pendulum extension	Impact velocity	3.9 m/s
Pendulum flexion	Impact velocity	3.9 m/s
Pendulum lateral	Impact velocity	3.5 m/s
Thorax		
Impactor frontal*	Impact velocity	4.3 m/s
	Impactor mass	3.8 kg
Impactor frontal*	Impact velocity	6.7 m/s
	Impactor mass	3.8 kg
Impactor lateral	Impact velocity	4.3 m/s
	Impactor mass	3.8 kg
Impactor lateral	Impact velocity	6.7 m/s
	Impactor mass	3.8 kg
Lumbar		
Pendulum frontal*	Impact velocity	4.4 m/s

* hardware dummy test data available

The frontal head drop test simulated a facial impact and was performed at two heights to evaluate the rate-dependency of the foam of the dummy head. The lateral head drop test simulated an impact of the dummy head under an angle with a side structure of a vehicle. The impacted plate was rigid. The acceleration of the head center of

gravity was computed. Simulation setups are shown in figure 3.

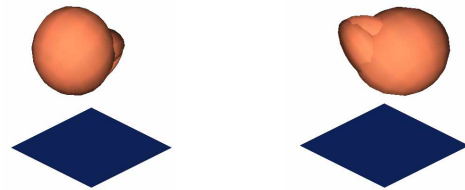


Figure 3. Simulation setup of Q3 head drop test in frontal (left) and lateral (right) direction.

The neck pendulum test was designed to evaluate the performance of the neck in three bending directions: flexion, extension and lateral flexion. The neck was disassembled from the dummy and mounted to a pendulum on the proximal side, while it was mounted to a standardized test mass representing a dummy head on the distal side, as shown in figure 4. The pendulum was stopped by a 3 inch layer of honeycomb, which was modeled in a contact characteristic with a crush force of 2500 N and 75% allowable compression. The velocity decrease of the pendulum and the total head rotation were computed.



Figure 4. Simulation setup of Q3 dummy neck pendulum test just before impact (left) and at time of maximum neck bending (right)

The thorax impactor test was designed to evaluate the thoracic response to impact in frontal and lateral direction. The free-flying impactor with a mass of 3.8 kg struck the sternum in frontal and the ribs in lateral impact at speeds of 4.3 m/s and 7.6 m/s. The thoracic response was characterized by a force-deflection plot for frontal impact and a force history plot for lateral impact. The simulation setups for thorax impactor tests are shown in figure 5.

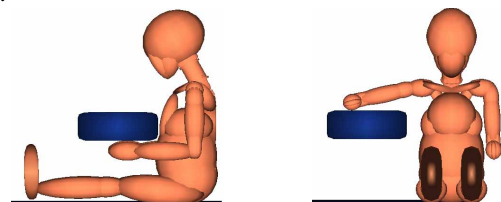


Figure 5. Simulation setup of Q3 dummy thorax impactor test in frontal (left) and lateral (right) direction

The lumbar pendulum test setup was similar to the neck pendulum test, where the neck assembly

was replaced by the lumbar spine assembly. The pendulum impact speed was increased from 3.9 m/s to 4.4 m/s. For an image of the test setup it is referred to the setup for the neck as shown in figure 4.

Q1.5 dummy model – To evaluate the Q1.5 dummy model response, simulations similar to those performed for the Q3 dummy model validation were setup. A smaller amount of tests was available for the Q1.5 dummy, as shown in table 4. Since the neck of the Q1.5 dummy and corresponding dummy model were identical to the neck of the Q3 dummy and corresponding model, no validation of the Q1.5 neck was performed. The mass of the thorax impactor was reduced from 3.8 kg to 2.6 kg, as prescribed in the dummy requirements [FTSS, 2003]. For head frontal drop, thorax frontal and lumbar flexion tests, hardware dummy test data was available in addition to dummy design requirements. For a more detailed description of the test setup it is referred to the Q3 dummy component validation paragraph.

Table 4: Overview of validation performed on Q1.5 dummy model.

Test description	Specifications	
Head		
Frontal drop*	Drop height	130 mm
Thorax		
Impactor frontal*	Impact velocity	4.3 m/s
	Impactor mass	2.6 kg
Impactor lateral	Impact velocity	4.3 m/s
	Impactor mass	2.6 kg
Impactor lateral	Impact velocity	6.7 m/s
	Impactor mass	2.6 kg
Lumbar		
Pendulum frontal*	Impact velocity	4.4 m/s

* hardware dummy test data available

Human child model development

Human child models of a 1.5 and a 3-year-old child were developed in order to be able to compare responses between the two human surrogate models. The models were developed by a scaling technique similar to the technique used for the development of the Q1.5 dummy model. The model was scaled from the MADYMO human occupant model in a 50th percentile male configuration [Happee, 2001]. Different from the ellipsoid dummy models, these models are characterized by a mesh representing the skin, by flexible bodies representing a fully deformable thorax and abdomen and by additional joint models representing all spinal flexibility.

The 35 anthropometric scaling parameters of the 50th percentile adult were derived from

RAMSIS anthropometric database [Seidl, 1994]. The anthropometry datasets for 1.5-year-old and 3-year-old were based on the design specifications of the Q3 and Q1.5 dummies, which were derived from the CANDAT child anthropometry database [Twisk, 1993]. Less important anthropometric parameters that were not available within CANDAT were taken from the GEBOD database [MADYMO, 2004]. These less important parameters were altered to improve the segment mass distribution resulting from the scaling routine. An overview of CANDAT mass specifications and resulting model segment mass distribution is given in table 5. The scaling routine optimization target included total dummy mass, which was reached. The models resulting from the scaling procedure are shown in figure 6.

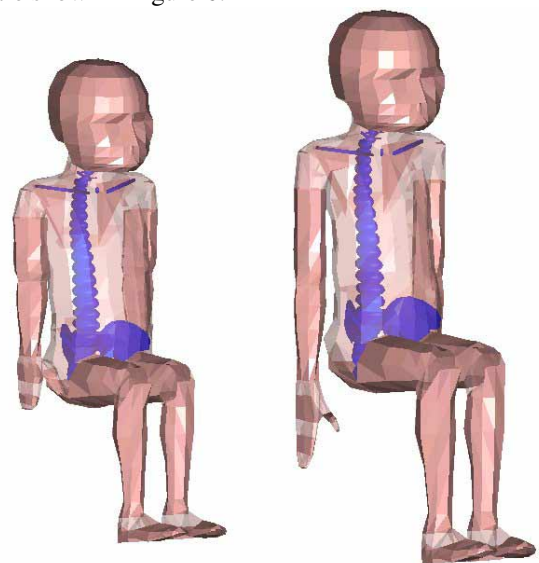


Figure 6. The MADYMO 1.5-year-old (left) and 3-year-old human child models.

Table 5: Segment mass distribution as specified in CANDAT database and as resulting from human models of 3-year-old and 1.5-year-old children.

Segment	3 yo model	3 yo specs.	1.5 yo model	1.5 yo specs.
Head	3190	3220	2510	2540
Neck	330	300	300	300
Torso	6220	6410	5120	5100
Arm upper	370	370	280	270
Arm lower	210	210	150	150
Hand	100	130	080	100
Thigh	950	980	580	570
Leg lower	500	500	300	290
Foot	250	240	170	160
Total	14500	14500	11020	11020

The developed human child models represented children of approximately 1.5 years and 3 years of

age. While the anthropometry was defined from anthropometric databases, the stiffness and damping parameters were scaled based on geometrical scaling on body part level and did not take structural changes and differences in material properties between children and adults into account.

Group I CRS simulation

All developed child models, Q1.5 and Q3, as well as human 1.5-year-old and 3-year-old, can be positioned in a Group I child restraint system (CRS). A Group I seat model positioned in a typical car seat was developed to evaluate the behavior of the developed child models in a typical vehicle crash environment.

A mesh of the outer geometry of a production CRS was generated and implemented in MADYMO. The finite element CRS was considered undeformable, while seat compliance was modeled by means of a contact characteristic between child model and CRS. The CRS was positioned in two planes with a contact characteristic representing a rear seat of a typical passenger car. The seat was mounted to the vehicle with the vehicle's three-point belt system, modeled by a multi-body belt. The child model, either human or dummy, was positioned on the CRS after which FE belts were wrapped around the child that represented the internal 5-point harness of the CRS. An image of a Q3 dummy model in the modeled CRS on the vehicle rear seat is shown in figure 7.

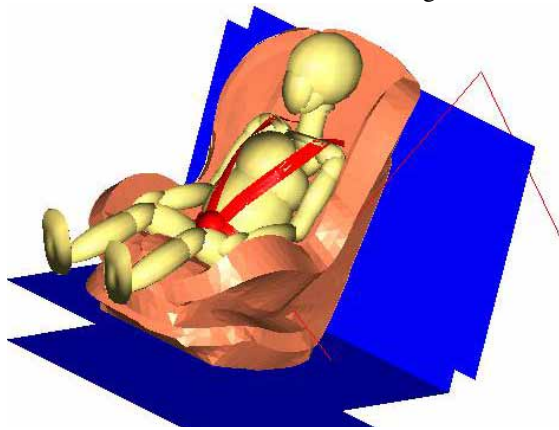


Figure 7. Generic child restraint model of Group I seat, mounted on vehicle rear seat with positioned Q3 dummy model and FE internal harness.

A frontal crash was simulated by prescribing an acceleration field to child model and CRS, while the vehicle seat was mounted to reference space. The supplied pulse was taken from ECE-R44 regulations [ECE, 1998]. Since the Q3 dummy is the proposed upper limit dummy for Group I CRS evaluation, simulations have been performed with

the Q3 dummy model and with the 3-year-old human model.

No experimental validation data was available to validate the CRS model or to evaluate the response of child dummy or human model in a full scale crash environment.

Injury Reference Values for 3-year-old children

Injury Reference Values (IRV) for a 3 year-old child are shown in table 6. IRV's indicate a reference value at which injury may occur. Some of these values have been defined in regulations [ECE, 1998], others are proposed values for regulations [Eppinger, 2000], some were scaled by body mass ratio from adult cadaveric data [Mertz and Patrick 1971, Cavanaugh 2002], while others were adapted from advanced scaled data [Ivarsson 2004, 2005]. The values presented here were meant to be mere indications of injury severity. They were used for ease of normalizing various responses, not to predict the occurrence of injury per se.

In order to present a normalized injury indicator, the relative Injury Reference Value (rIRV) was defined as follows:

$$rIRV = \frac{response}{IRV} \quad (1)$$

Table 6: Injury Reference Values (IRV) of 3-year-old children with source and subsequent comment.

Criterion	IRV	Source
Head Injury Crit. HIC	570	<i>Eppinger 2000</i>
Head Excursion	0.55 m	<i>ECE-R44</i>
Neck Injury Predict., tension-extension Nij TE	1	<i>Eppinger 2000</i>
Neck Injury Predict., compression-ext. Nij CE	1	<i>Eppinger 2000</i>
Neck Lower Force, lateral shear Fy	273 N	<i>Mertz and Patrick 1971, mass scaled</i>
Neck Lower Force, axial Fz	-1380 N	<i>Eppinger 2000</i>
Neck Lower Moment, lateral bending Mx	16.5 Nm	<i>Ivarsson 2005, Nij intercept</i>
Sternum Displacement	0.034 m	<i>Eppinger 2000</i>
Thorax Viscous Criterion VCmax	0.74	<i>Cavanaugh 2002, mass scaled</i>

Hence, the model response divided by the in table 6 defined IRV is a normalized measure for injury potential and was used as such in presenting results. When rIRV equals 1, the computed response is equal to the IRV defined.

Posture study

A posture study was performed since it was hypothesized that children rarely sit in the same posture for a long period. At first, a real-world photo study was performed to indicate which posture children regularly take on longer drives. The resulting most common or most extreme postures were then simulated with a Q3 dummy model and a 3-year-old human model in a Group I seat at ECE-R44 impact level.

Real-world photo study – To investigate what postures children seated in Group I seats take on long drives, parents of a total number of 10 children were asked to take pictures of their children and to fill in a questionnaire. Three series of photos were taken.

- **A:** one picture of the child in the CRS every 15 minutes during drives of at least one hour, taken by the co-driver.
- **B:** one picture of the child just after it was positioned in the CRS and one right after the drive, so that the picture could be taken from outside the vehicle to obtain a better view.
- **C:** pictures of the child when it was observed that it took a strange or extreme position.

The resulting photographs were organized into two categories. First of all, in order to find common postures that often occurred and that many children took. Secondly, in order to find some extreme postures that children take, which are potentially dangerous in case of a crash.

Modeling of poses – To evaluate the effect of various poses or postures, some of the observed postures were simulated in the CRS on the vehicle rear seat model environment that was developed within this study. By changing the positions and orientations of the kinematic joints of dummy and human model the postures observed in the photo study could be modeled. With the changed position also the belt routing changed, which made rewiring of the FE internal CRS harness necessary.

The Q3 dummy model joint characteristics needed to be changed in order to be able to position the dummy in many of the postures. Most dummy joints provide resistance to any position other than the reference position, which in the modeling environment with the original dummy model resulted in a transient effect at the start of the simulations, where the joint relaxed into its reference state. In order to eliminate this undesired transient effect, the dummy joint characteristics were altered so that no force or torque was generated at the desired joint orientation. This increase of range of motion of dummy joints,

reduced the quality of validation of the model. However, the effect on dummy response was found to be small and acceptable for performing trend studies.

RESULTS

The results from this study consist of the simulation responses from the dummy component tests and the response of the generic CRS model simulations, followed by results from the photo study and the numerical analysis on the various postures.

Dummy model component validation

The component validation results of both Q3 and Q1.5 dummy models will be presented in this section. Additional figures can be found in appendix 1 and 2 for Q3 and Q1.5 respectively.

Q3 head – The validation of the Q3 dummy head in frontal drop test at 130 mm was compared with three hardware dummy tests, as shown in figure 8. The x-acceleration of the head was higher than observed in any of the three experiments, which indicated that the head contact stiffness was too high in the model. However, the maximum resultant acceleration was 1254 m/s^2 , which fulfilled the requirement that the acceleration should lie in between 981 and 1275 m/s^2 . At a drop height of 376 mm the model response was slightly lower than the hardware dummy responses. The lateral drop test at 130 mm drop height showed that the model fulfilled the requirement of minimum 1177 m/s^2 and maximum 1472 m/s^2 at a resultant head acceleration of 1257 m/s^2 . At 200 mm drop height, the model response was comparable to the test responses.

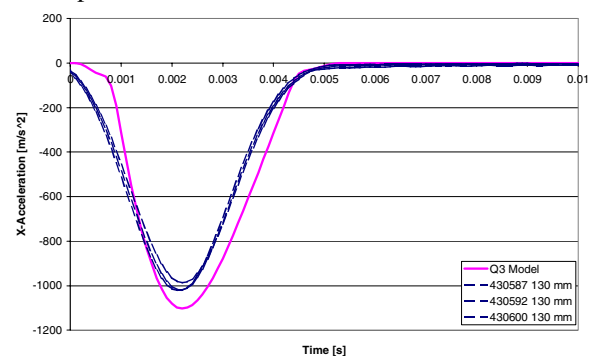


Figure 8. X-acceleration of Q3 head frontal drop test validation at 130 mm height.

Q3 neck – Validation of the neck of the model in flexion resulted in a plot of pendulum velocity decrease, as shown in figure 9, and in total head rotation, as shown in figure 10. The velocity decrease plot showed that the pendulum speed decreased slightly more rapid than allowed by the

corridor. The total head rotation was slightly higher than allowed by the dummy requirements and the angular rate of the neck was slightly lower, as shown by the peak occurring later than allowed by the bounding box.

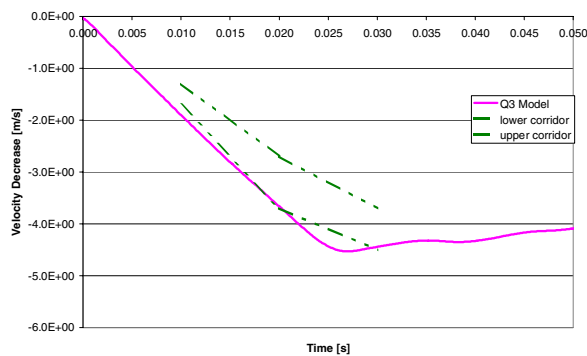


Figure 9. Velocity decrease of Q3 neck flexion pendulum test validation at 3.9 m/s impact speed.

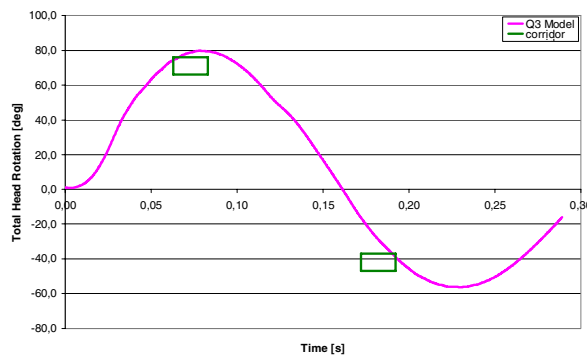


Figure 10. Total head rotation of Q3 neck flexion pendulum test validation at 3.9 m/s impact speed.

The results of the neck pendulum tests in the other loading directions, extension and lateral flexion, showed similar results. The velocity decrease was on the high side of the corridor, while the maximum allowable head rotation was slightly larger and occurred slightly later than the maximum set in the requirements.

Q3 thorax – The thoracic response of the Q3 model was evaluated with the force-deflection response resulting from the frontal thoracic impactor test, as shown in figure 11. The hardware dummy showed a stiffer performance than the corridor, on which it is elaborated by de Jager et al. [de Jager, 2005]. The model response resulted in an even higher impact force and a maximum deflection close to 30 mm. A similar trend was observed at higher impact speed of 6.7 m/s. The odd shaped fluctuation of the model response was attributed to a vibration in the impactor force history, which indicated a lack of damping in the dummy model.

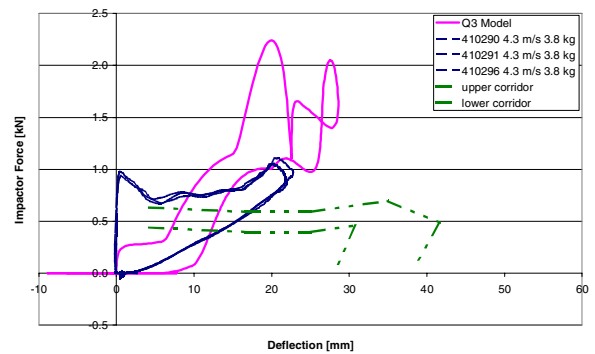


Figure 11. Force-deflection of Q3 thorax frontal impactor test at 4.3 m/s with 3.8 kg mass.

The lateral thoracic force response was approximately four times higher than defined in the corridor, while timing was fairly correct, as figure 12 indicates.

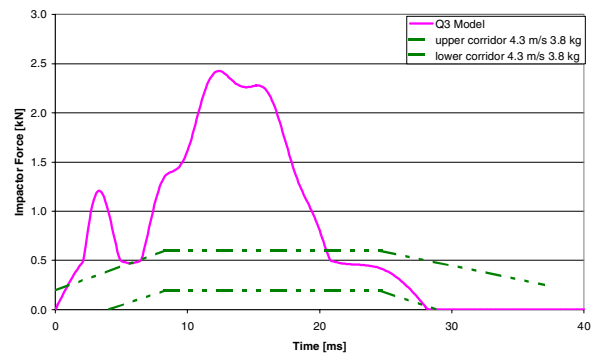


Figure 12. Force history of Q3 thorax lateral impactor test at 4.3 m/s with 3.8 kg mass.

Q3 lumbar – The lumbar pendulum test results are plotted in figures 13 and 14. The model response was very similar to the three hardware dummy test responses, but the bounding boxes for maximum total head rotation and timing of maximum total head rotation were not completely met.

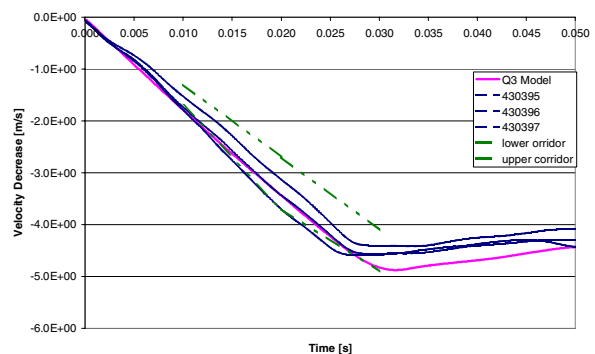


Figure 13. Velocity decrease of Q3 lumbar flexion pendulum test validation at 4.4 m/s impact speed.

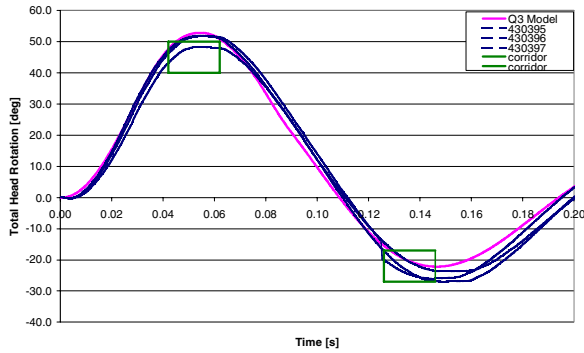


Figure 14. Total head rotation of Q3 lumbar flexion pendulum test validation at 4.4 m/s impact speed.

From the Q3 dummy model component validation it was concluded that the model response did not always meet the requirements. However, most of the responses fell only slightly outside the corridor, except for thoracic force response that was approximately four times higher than required.

Q1.5 head – The x-acceleration response of the head frontal drop test at 130 mm for the Q1.5 dummy model is shown in figure 15. The model response was about 15 % higher than the hardware dummy response. Also, the timing of the peak acceleration occurred slightly earlier. The resultant head acceleration fell inside the requirement of $1089 \pm 284 \text{ m/s}^2$ at 1299 m/s^2 .

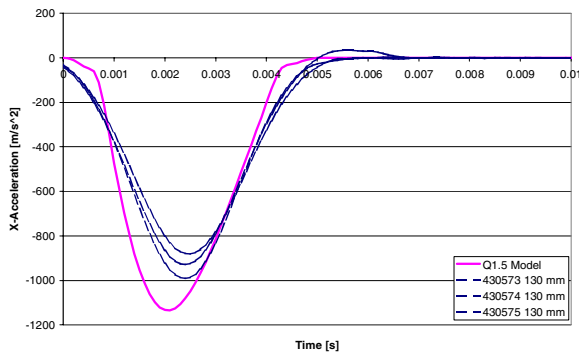


Figure 15. X-acceleration of Q1.5 head frontal drop test validation at 130 mm height.

Q1.5 thorax – The frontal thoracic impactor response of the 4.3 m/s test is plotted in figure 16. The hardware dummy performance is slightly different from the corridor, on which it is referred to de Jager et al. [de Jager, 2005]. The force response of the model was about four times higher than the corridor, while the maximum deflection did not increase up to the range set in the corridor. Lateral thoracic tests resulted in a similar trend, where the force was approximately four times higher for both high and low impact speed tests.

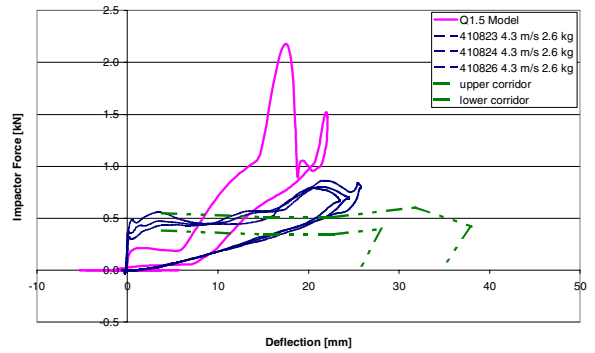


Figure 16. Force-deflection of Q1.5 thorax frontal impactor test at 4.3 m/s with 2.6 kg mass.

Q1.5 lumbar – The lumbar pendulum test results are shown in figures 17 and 18. While the pendulum velocity decrease of the model fell inside the corridor during the larger part of the simulation, the maximum total head rotation was larger than allowed by the requirements. Nevertheless, the timing was correct and the model response was very similar to the hardware dummy response.

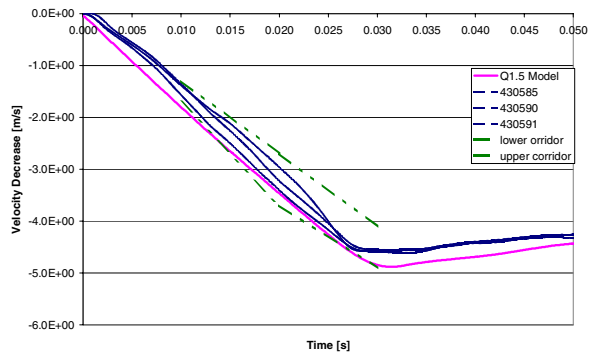


Figure 17. Velocity decrease of Q1.5 lumbar flexion pendulum test validation at 4.4 m/s impact speed.

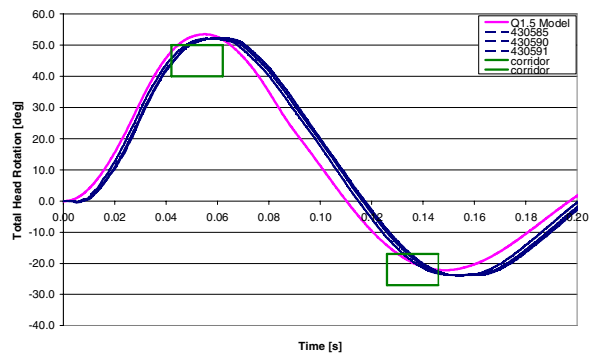


Figure 18. Total head rotation of Q1.5 lumbar flexion pendulum test validation at 4.4 m/s impact speed.

From the Q1.5 dummy component validation simulations it was concluded that similar trends were observed as in Q3 component validation. The model response met the requirements or just did not meet the requirements for most all responses, except for thoracic impactor force response.

Group I CRS simulation

Kinematic simulation results of the Q3 dummy model and 3-year-old human child model seated in a Group I CRS at ECE-R44 impact are shown in figure 21. At first, the CRS and child model moved forward. After 50 ms the lower neck went into flexion, while the upper neck went into extension, caused by the unrestrained head moving relative to the restrained torso. At 100 ms after impact a difference between dummy and human was observed. The dummy allowed more forward movement of the shoulder than the human model. The human model's shoulder was restrained more. Therefore, later in the event, the human torso stayed more upright than the dummy torso. Even though the belt friction coefficient was identical at 0.4, differences in the contact algorithms between ellipsoid and rigid FE models might have caused this. The kinematics of head and neck was fairly similar throughout the rest of the event.

A comparison of model response in terms of resultant head acceleration between Q3 dummy model and human model, as shown in figure 19, indicated that both timing and maximum value of head acceleration were fairly similar between human and dummy model.

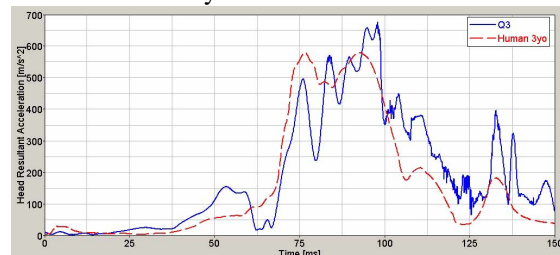


Figure 19. Head resultant acceleration of Q3 dummy model and human 3-year-old model in Group I seat with ECE-R44 pulse.

In terms of force response, the axial force generated in the lower neck indicated that both dummy and human model predict neck tension at first and neck compression later in the event, as figure 20 shows. The maximum compressive force in the lower neck is similar for both at around -1500 N.

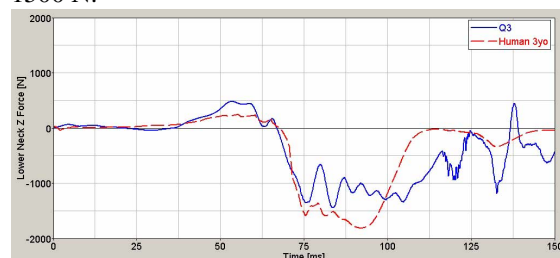


Figure 20. Lower neck axial force of Q3 dummy model and human 3-year-old model in Group I seat with ECE-R44 pulse.

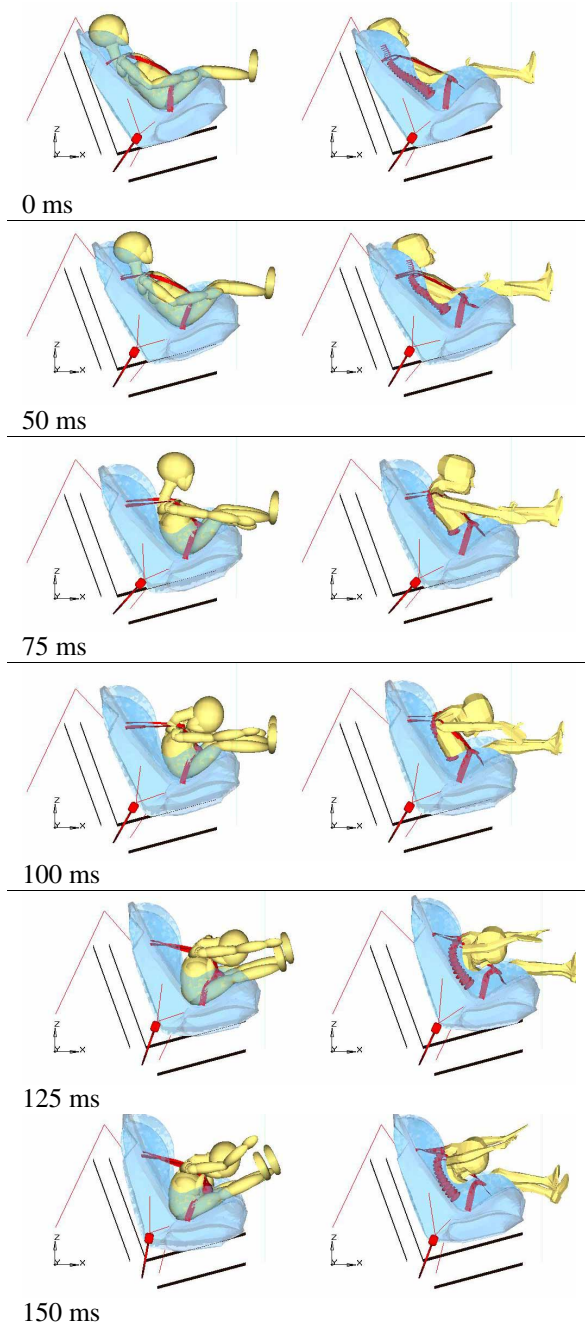


Figure 21. Simulation of Q3 dummy model (left) and human 3-year-old model (right) in Group I seat with ECE-R44 pulse.

In order to quickly compare the effect of a certain impact configuration on the model response, in figure 22 the relative Injury Reference Values (rIRV), as defined in table 6, for the performed simulations are shown. From the Q3 model and human 3-year-old model comparable rIRV values were computed for HIC and head excursion. The values for N_{ij} in the human model simulation were far lower than the Q3 model, due to almost non-existing extension in the human model upper neck. Forces and moments in the lower neck were comparable. Large differences existed for the sternum displacement and VCmax

as well. The lower dummy sternum displacement matched with the low sternum displacement observed in thoracic impactor simulations, as shown in figure 11.

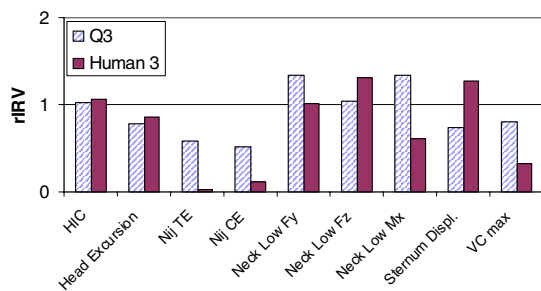


Figure 22. Relative Injury Reference Values (rIRV) of simulations with Q3 dummy model and human 3-year-old model in Group I seat with ECE-R44 pulse.

Real-world photo study on poses

The photo study resulted in a total of 141 photographs. A division was made between children based on age and weight. Four out of ten children were best represented by a 3-year-old model, while the other six were best represented by a 1.5-year-old model. Obviously, a younger child has more freedom of movement in its seat. As a result, a larger variety of postures was found for smaller children.

The standard posture, sitting up straight, was found most often. This posture is shown in figure 23 on the left. An extreme posture is shown in figure 23 on the right. The child in the 1.5-year-old group was slouched and managed to hold her feet in her hands.

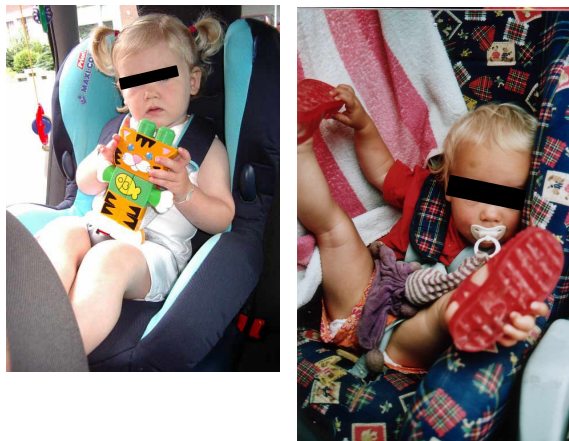


Figure 23. Photo of child sitting straight up (left) and of child holding her feet in her hands (right).

Often, children were hanging to either one side of their CRS, resting their heads on the wings of the CRS. This posture is shown in figure 24 on the left. Either the whole body was slanted, or just the

neck was laterally flexed. The child's neck was often hanging in the shoulder belt. A posture typical for older children was to stretch one of their legs against the front row seat, as shown in figure 24 on the right. Often this was combined with the other limb pulled up and resting on the knee of the stretched limb. In order to reach the front row seat with their feet, children were often slouched in their CRS.



Figure 24. Photo of child sleeping slanted (left) and of child stretched out, one leg pulled up and right foot against front seat (right).

An uncommon position, but observed with two children, was to escape from the shoulder harness and then lean forward. The parents of these specific children stated clearly that they removed all slack from the internal harness system during installation, but the child still managed to escape. A photo of this position is shown in figure 25.



Figure 25. Photo of child escaped from shoulder belts.

Additionally to these five poses, children were sometimes leaning forward in their shoulder restraint, completely hunched. At other times, children managed to escape from their shoulder harness and rotate their whole body so that they could look backward. Many variations on all poses existed as well.

Modeling of poses

The five poses shown in figures 23-25 were chosen to be modeled in the Group I CRS simulation environment discussed before. Simulations were performed with both the Q3 as well as the 3-year-old human model.

Standard pose – The standard pose, of a child sitting straight up, was considered to be identical to the standard model setup that was discussed earlier. This posture and the accompanying model are referred to as the base posture and model in the following figures.

Child holding feet in her hands – The pose of a child holding her feet in her hands, was modeled by changing the orientation of the joints such that all extremities were stretched and the hands were in the proximity of the feet. The child model was positioned somewhat slouched in its seat. The initial setup is shown in figure 26. While in reality this pose was observed at a child representing the 1.5-year-old age group, simulations were performed with the 3-year-old child models.

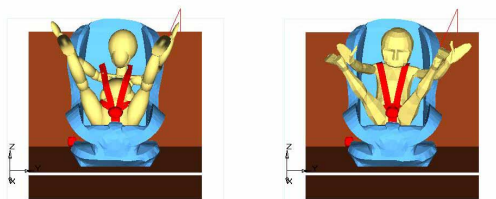


Figure 26. Simulation setup of Q3 dummy model (left) and human 3-year-old model (right) holding feet in hands.

The resulting kinematic response consisted of upper and lower limbs flinging in the direction of the force vector, e.g. frontal. This behavior was observed in the standard posture as well, only with a different initial orientation of the limbs. The kinematic response is therefore similar to the standard posture response.

Child sleeping slanted – The child sleeping slanted in the CRS was modeled by rotating the body slightly and by adding lateral flexion in the neck, as shown in figure 27. The left shoulder belt was proximal to the neck, causing an asymmetric load condition.

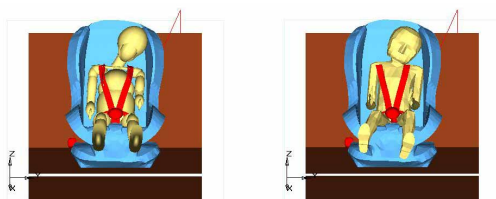


Figure 27. Simulation setup of Q3 dummy model (left) and human 3-year-old model (right) sleeping slanted.

The kinematic simulation results, shown in figure 28 at 95 ms after impact, showed that the asymmetric load condition resulted in lateral components of head movement.

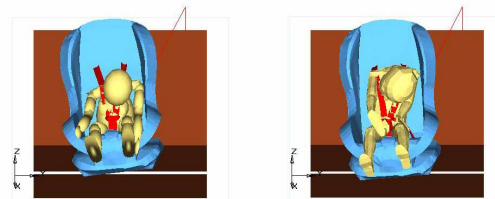


Figure 28. Simulation of Q3 dummy model (left) and human 3-year-old model (right) sleeping slanted, 95 ms after impact.

Child with one leg stretched against front row seat – In order to simulate the effect of a front row seat on the child's lower extremity response, a plane was added with an assumed contact stiffness characteristic for a seat back. Initially, the right lower limb of the child was stretched and in contact with the plane. The left limb was pulled up with the left foot resting on the right knee. This setup is shown in figure 29. Additionally, the child was slanted causing an asymmetric load condition at the shoulder harness.

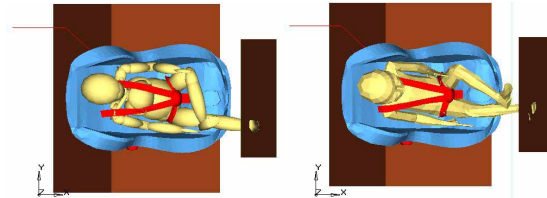


Figure 29. Simulation setup of Q3 dummy model (left) and human 3-year-old model (right) stretched out, one leg pulled up and right foot against front seat.

In figure 30 the simulation results are shown at 85 ms after impact. The simulation results were similar to those of the standard position, except for the lower extremities that did not stretch out but were compressed against the seat, inducing knee flexion. The forces generated in the tibia were at 400 N well below the fracture threshold defined from scaled adult data at 1860 N [Ivarsson, 2005]. However, in the current simulation setup knee flexion was present, while in reality a fully extended knee might induce higher forces in the lower extremity.

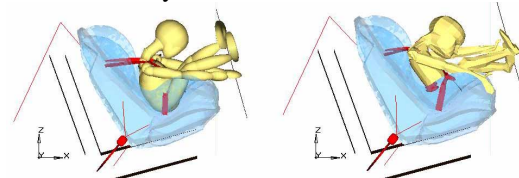


Figure 30. Simulation of Q3 dummy model (left) and human 3-year-old model (right) stretched out, one leg pulled up and right foot against front seat, 85 ms after impact.

Child that escaped from shoulder belts – The child that escaped from the shoulder harness and then leaned forward was modeled as shown in figure 31. The FE internal harness was routed differently, with the shoulder belt going underneath the armpits.

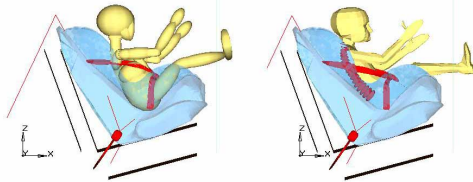


Figure 31. Simulation setup of Q3 dummy model (left) and human 3-year-old model (right) escaped from shoulder belts.

Simulation results of the child that escaped from the shoulder belts are shown in figure 32. The child was correctly restrained by the lap belt of the harness and therefore full body excursion relative to the CRS did not occur. However, the unrestrained upper torso, head and neck moved forward causing large lumbar flexion and the dummy spine being lined up with the force vector from the impact. The head excursion limit was exceeded. In a full-scale setup the head would have impacted the front row seat, possibly implicating severe head injury. However, this was not modeled since the Head Injury Criterion (HIC) is very sensitive to the contact stiffness of the front row seat, for which no validated model was available.

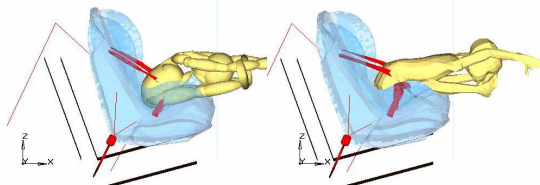


Figure 32. Simulation of Q3 dummy model (left) and human 3-year-old model (right) escaped from shoulder belts, 120 ms after impact.

Injury criteria of modeled poses – The effect of various poses on the response of a child model was evaluated in terms of relative injury reference values. The N_{ij} value in compression-extension mode was higher than in the base or standard case for two postures; feet in hand and sleeping slanted. At both these postures the body was slouched, resulting in a changed neck orientation with respect to the impact direction. The changed orientation caused a different loading condition at the upper neck, where N_{ij} was computed.

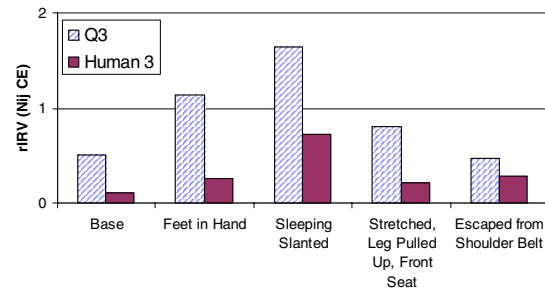


Figure 33. Relative Injury Reference Values (rIRV) of N_{ij} compression-extension of simulations with Q3 dummy model and human 3-year-old model in Group I seat with ECE-R44 pulse at different poses.

The head excursion rIRV was similar for all simulations except for the simulation where the child escaped from the shoulder belts. There, the ECE-R44 excursion limit was exceeded for both dummy and human model. The human model exceeded the head excursion limit more than the dummy model, which was caused by the spinal elongation that can be observed in figure 32. Due to the absence of a front row structure in an ECE-R44 setup, as well as in the current simulation setup, the effect of exceeding the head excursion limit was not quantified. However, high head accelerations and neck loads are likely to occur.

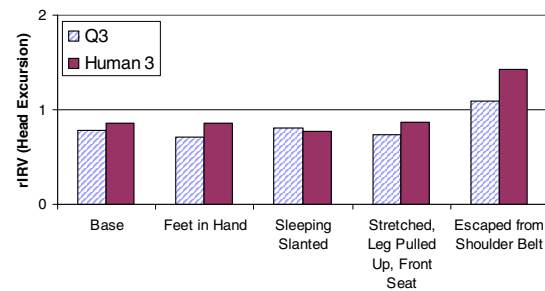


Figure 34. Relative Injury Reference Values (rIRV) of head excursion of simulations with Q3 dummy model and human 3-year-old model in Group I seat with ECE-R44 pulse at different poses.

Due to the asymmetric loading condition, lateral motion and computed forces and moments were expected to occur. Two postures where the body was slanted and the neck was laterally flexed initially were the child sleeping slanted and the child with one leg stretched against the front row seat. For these two simulations a large lateral shear force in the lower neck was observed, as shown in figure 35. The forces were up to two times higher than observed in the base model and were also twice as high as the IRV.

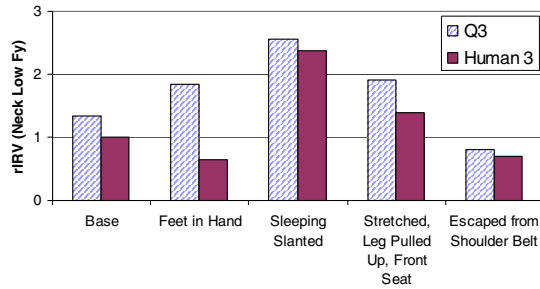


Figure 35. Relative Injury Reference Values (rIRV) of lower neck lateral shear force of simulations with Q3 dummy model and human 3-year-old model in Group I seat with ECE-R44 pulse at different poses.

In order to further investigate the occurrence of lateral loading, the lateral bending moment in the human model neck is plotted for all poses in figure 36. Lateral neck bending occurs in the base model, due to the asymmetric mounting configuration of the CRS on the test bench by means of a three-point belt restraint. However, when additional asymmetry was introduced by slanting the human child model, the lateral bending moments that occurred in the lower neck were up to twice as high and exceeded the IRV for lateral neck moment that was defined at 16.5 Nm in table 6.

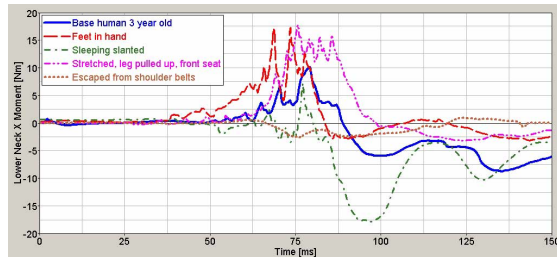


Figure 36. Lower neck lateral bending moment of simulations human 3-year-old model in Group I seat with ECE-R44 pulse at different poses.

The results from the different poses indicated that loading levels were not dramatically different from a properly restrained child. However, the simulation of the child that escaped from the shoulder belt exceeded the head excursion limit. A child that was not symmetric relative to the shoulder restraint sustained lateral forces and moments in the neck of a level that might potentially induce injury.

DISCUSSION

The development of the Q3 dummy model, based on the pre-existing model, resulted in a model that showed comparable results with respect to hardware dummy tests. Additionally, the design requirements for the dummies were met or almost met for all tests except for the thoracic impactor

tests. The thorax of the model was consistently stiffer than the corridors. This resulted in forces that were approximately 4 times higher than required at deflections lower than required. Improvements to the dummy model thorax are necessary in order to show a similar response to the hardware dummy. The need to fit the thorax corridors is subject to discussion since these corridors were developed based on scaling from cadaveric adult data, an approach that involved a large number of assumptions.

Q1.5 dummy development through anthropometrical scaling was a useful process in scaling the outer dimensions of the dummy. The stiffness properties of contact characteristics and joint resistance models were scaled accordingly. The latter approach was validated by the component simulations in which the stiffness characteristics were tested. Manual adaptations were necessary in order to achieve a correct segment mass distribution, since the MADYMO/Scaler routine did not scale based on those. Component validation showed that the developed Q1.5 model response fell inside or was just outside the requirements, except for the thorax. The lack of thorax validation was a direct consequence of the scaling approach used to develop the dummy from the Q3 model. It must be stated however, that the amount of tests performed was limited.

The developed human child models were scaled from an adult anthropometry. The resulting models met anthropometrical requirements from the CANDAT database. However, the procedure involved large scaling ratios in which the potential for errors in scaling the various stiffness and force models was large. Within the current human child model development, structural differences between humans and children and variation of material properties by age were not taken into account. For example, the long bones of children have growth plates and their bone tissue is generally more elastic than that of adults [Ivarsson, 2004]. In an FE environment these structural and material differences between children and adults can be taken into account intrinsically [Okamoto, 2002], while in a multi-body environment they can be taken into account by using more advanced scaling techniques, incorporating additional joints and material properties.

Validation of human child models was not performed in this study. Since cadaveric child data is unavailable due to ethical considerations, validation needs to be performed differently. A possible approach in validating a human model can be to perform crash reconstruction. Correlation data between impact severity and resulting injuries is

often available in detailed car crash databases, also for children. When a large number of crashes are simulated and the computed injury criteria from the human model match up with the injuries recorded in the medical records, confidence in the injury predictive capacity of the human models can be achieved. In a first attempt to validate the human child models, in this paper the response of the validated Q3 model was compared with the 3-year-old child human model. Most responses were similar. However, large differences existed in upper neck extension moment and in sternum displacement.

In the posture study, the dummy model was applied for conditions it was not developed for. The extreme joint orientations resulted in transient effects at the beginning of the simulation. As a result model adaptations were necessary. The human model could be positioned in any of the postures without these transient effects, due to larger ranges of motion in the joints. The model response in the full scale CRS environment was comparable between human and dummy model, which indicated that both dummy and human model were valid tools to perform this type of investigation. No validation data was available for the CRS itself and for the human and dummy model in a full scale environment and therefore the results from this study should be considered as indications of trends that might occur in various poses.

In many of the most common poses the body was slanted, which caused an asymmetrical loading condition at the shoulder belts. This involved lateral movement of the head and lateral forces and moments in the neck of a level that is potentially hazardous. When a child was escaped from its shoulder belt restraint, the ECE-R44 criterion for head excursion was exceeded. Besides large axial forces in the spine, impact with a front seat can cause severe head and neck injuries.

CONCLUSIONS

From this study the following conclusions were drawn:

- The Q3 model update was validated against component test data and met the corridors, except for the thoracic response, which was approximately four times too stiff.
- The Q1.5 model, developed through anthropometrical scaling, largely fulfilled the dummy design requirements, again except for thoracic response
- The human child models were developed based on anthropometrical scaling, which resulted in human models resembling a 1.5 and a 3-year-old from CANDAT database.

- A posture study showed that children tend to move around in their CRS on longer drives, resulting in slanted and slouched positions.
- Correctly restrained children in a Group I seat were able to escape from their shoulder restraint, which increases risk of injury.
- Simulation of the various poses with the above discussed human surrogate models indicated that lateral neck loads were twice as high in slanting positions. Slouching resulted in higher neck loads as well.
- The simulation of the child that escaped from the shoulder belt was shown to be hazardous since the head excursion limit was exceeded by over 20 cm.
- Virtual testing was shown to be a useful method to investigate the types of crash conditions that may occur in the field, but that are difficult to test in an experimental environment.

ACKNOWLEDGEMENTS

The authors would like to acknowledge Westeinde Hospital in The Hague for the use of their CT scanner.

REFERENCES

Cavanaugh, J., "Biomechanics of Thoracic Trauma", in *Accidental Injury*, ed. Nahum and Melvin, Springer, 2002

ECE-Regulation 44. "Uniform Provisions Concerning the Approval of Restraining Devices for Child Occupants of Power-Driven Vehicles ("Child Restraint System")", Version 03, United Nations, 5th June 1998

Eppinger, R., Sun, E., Kuppa, S., Saul, R., "Supplement: Development of the Improved Injury Criteria for the Assessment of Advanced Automotive Restraint Systems – II", 2000, http://www-nrd.nhtsa.dot.gov/pdf/nrd-11/airbags/finalrule_all.pdf (accessed February 24 2005)

EU, "Community Road Accident Database", 2005, http://europa.eu.int/comm/transport/care/statistics/most_recent/detailed_breakdown/index_en.htm (accessed February 24 2005)

FTSS, "Q3 dummy design requirements document", First Technology Safety Systems, 2003

Happee, R., Ridella, S., Nayef, A., Morsink, P., Lange, R. de, Bours, R., Hoof, J. van, "Mathematical Human Body Models Representing a Mid Size Male and A Small Female for Frontal ,

Lateral and Rearward Impact Loading”, IRCOBI Conference, 2001

Ivarsson, J., Madeley, J., Crandall, J., Okamoto, M., Takahashi, Y., “Lateral Pedestrian Injury Criteria for the 6-year-old Child”, Society of Automotive Engineers (SAE), 2004

Ivarsson, J., “Personal Communication on Injury Criteria for the 3-year-old Child”, 2005

Jager, K. de, Ratingen, M. van, Lesire, P., Guillemot, H., Pastor, C., Schnottale, B., Tejera, G., Lepretre, J-P, “Assessing New Child Dummies and Criteria for Child Occupant Protection”, ESV Conference, 2005

MADYMO, “MADYMO v6.2 manuals”, Delft, The Netherlands, 2004

Meissner, U., Stephens, F., Alfredson, L., “Children in Restraints”, AAAM conference, 1994

Mertz, H., Patrick, L., “Strength and Response of the Human Neck”, Stapp Conference, 1971

Mimics 8.11 homepage, “http://www.materialise.com/mimics/main_ENG.html” (accessed February 24 2005)

Okamoto, M., Takahashi, Y., Mori, F., Hitosugi, M., Madeley, J., Ivarsson, J., Crandall, J., “Development of Finite Element Model for Child Pedestrian Protection”, ESV Conference, 2003

Quintero Del Rio, “A Survey of Parental Knowledge about Car Seats in Children”, Bol. Assoc. Med. P. R., 89(1-3):12-4, 1997

Seidl, A., “Das Menschmodell RAMSIS: Analyse, Synthese und Simulation dreidimensionaler Körperhaltungen des Menschen”, PhD-thesis Technische Universität München, 1994

Twisk, D., Beusenbergh, M., “Anthropometry of Children for Dummy Design” ECOSA Product Safety Conference, Amsterdam, 1993

APPENDIX 1: Q3 component validation

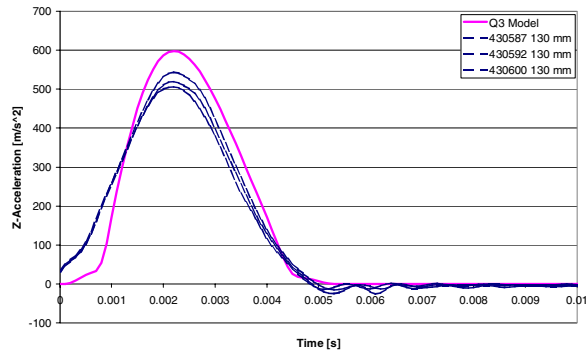


Figure 37. Z-acceleration of Q3 head frontal drop test validation at 130 mm height.

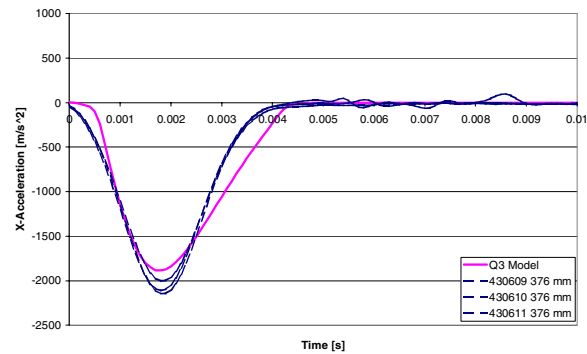


Figure 38. X-acceleration of Q3 head frontal drop test validation at 376 mm height.

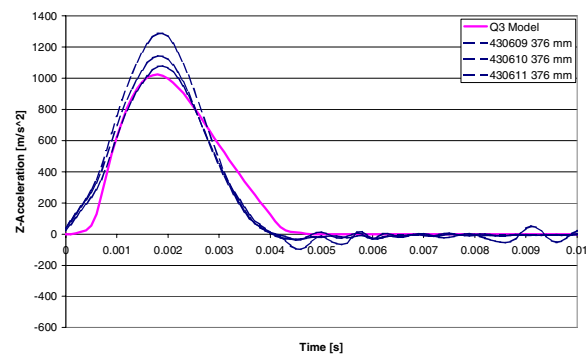


Figure 39. Z-acceleration of Q3 head frontal drop test validation at 376 mm height.

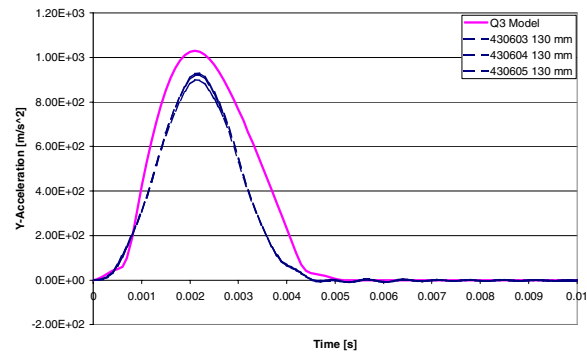


Figure 40. Y-acceleration of Q3 head lateral drop test validation at 130 mm height.

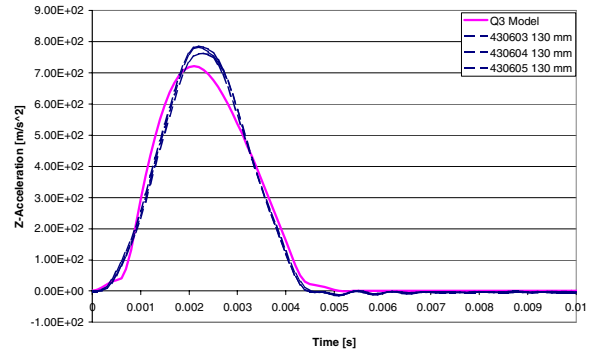


Figure 41. Z-acceleration of Q3 head lateral drop test validation at 130 mm height.

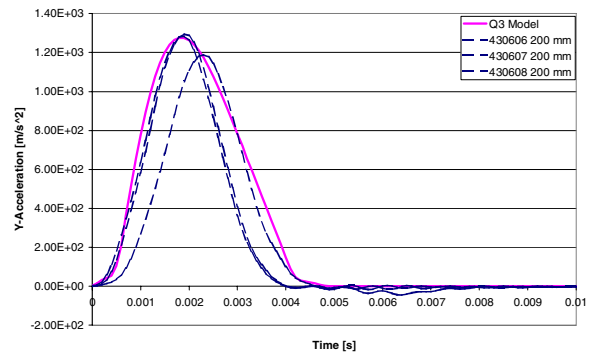


Figure 42. Y-acceleration of Q3 head lateral drop test validation at 200 mm height.

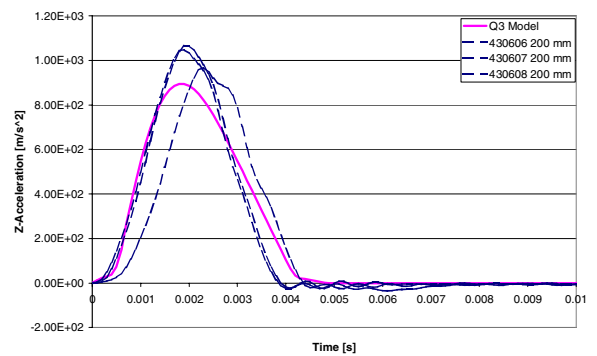


Figure 43. Z-acceleration of Q3 head lateral drop test validation at 200 mm height.

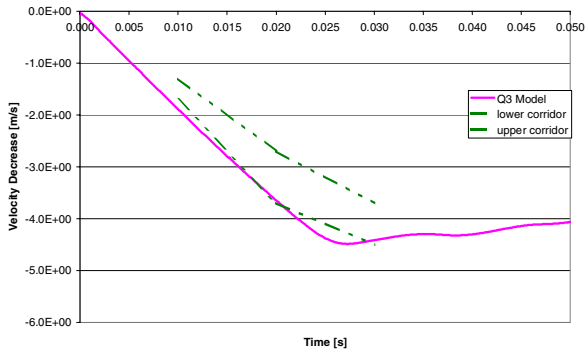


Figure 44. Velocity decrease of Q3 neck extension pendulum test validation at 3.9 m/s impact speed.

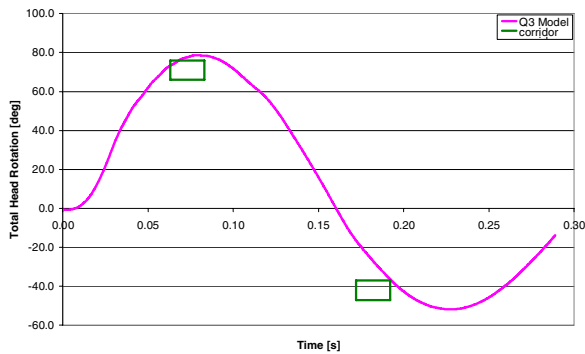


Figure 45. Total head rotation of Q3 neck extension pendulum test validation at 3.9 m/s impact speed.

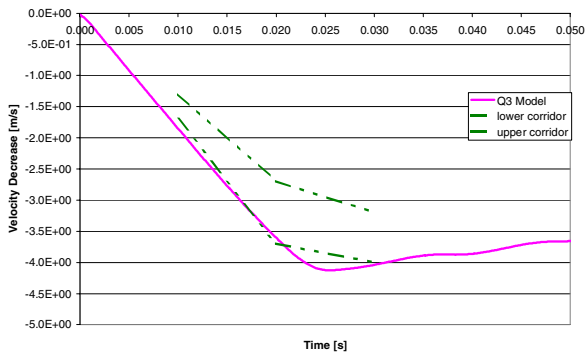


Figure 46. Velocity decrease of Q3 neck lateral flexion pendulum test validation at 3.9 m/s impact speed.

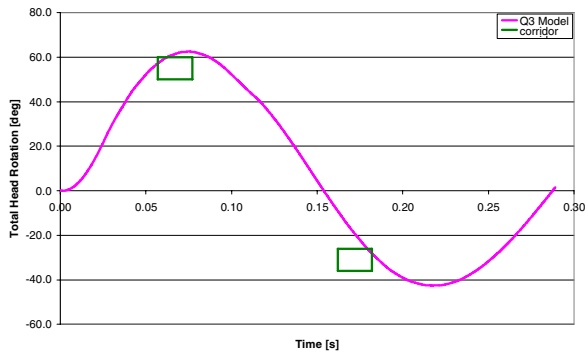


Figure 47. Total head rotation of Q3 neck lateral flexion pendulum test validation at 3.9 m/s impact speed.

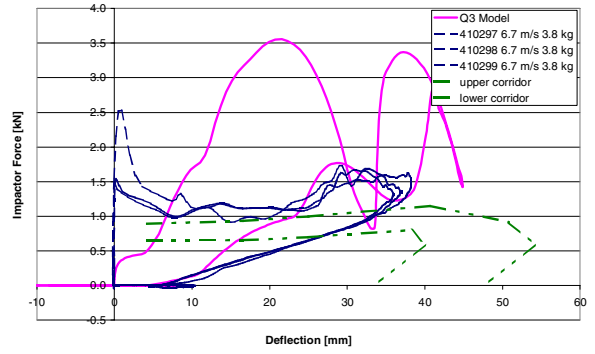


Figure 48. Force-deflection of Q3 thorax frontal impactor test at 6.7 m/s with 3.8 kg mass.

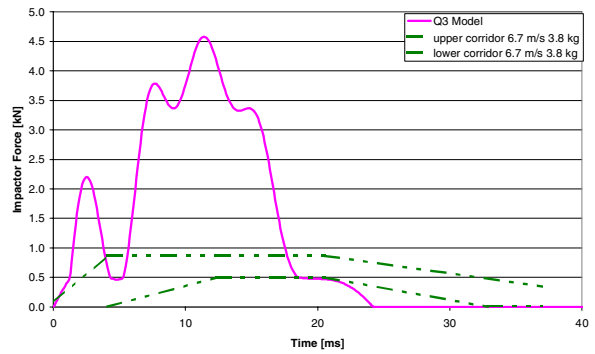


Figure 49. Force history of Q3 thorax lateral impactor test at 6.7 m/s with 3.8 kg mass.

APPENDIX 2: Q1.5 component validation

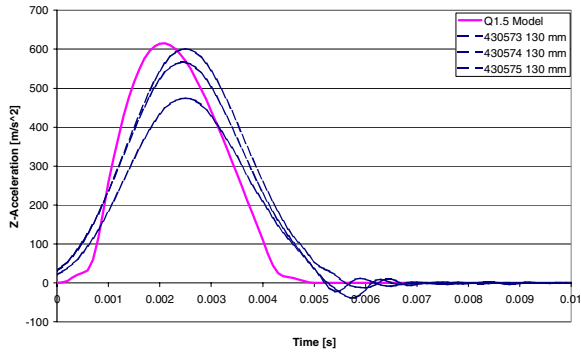


Figure 50. Z-acceleration of Q1.5 head frontal drop test validation at 130 mm height.

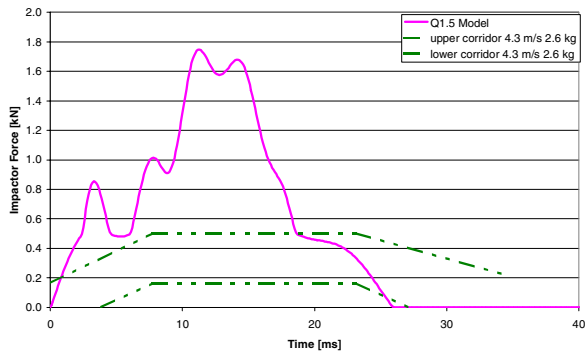


Figure 51. Force history of Q1.5 thorax lateral impactor test at 4.3 m/s with 2.6 kg mass.

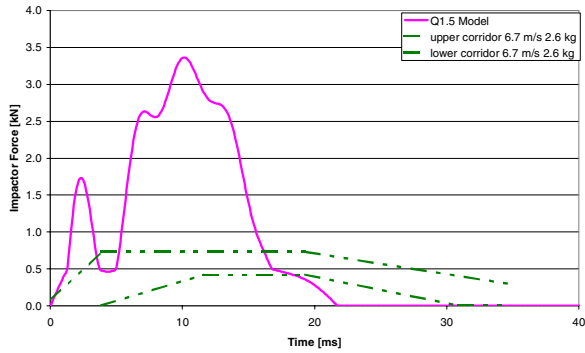


Figure 52. Force history of Q1.5 thorax lateral impactor test at 6.7 m/s with 2.6 kg mass.